Pure appl. geophys. 166 (2009) 2021–2035
0033–4553/09/122021–15
DOI 10.1007/s00024-009-0531-0

Pure and Applied Geophysics

Quantitative Interpretation of Self-Potential Anomalies of Some Simple Geometric Bodies

E. M. Abdelrahman,[1] K. S. Soliman,[1] E. R. Abo-Ezz,[1] K. S. Essa,[1] and T. M. El-Araby[1]

Abstract—We have developed a new numerical method to determine the shape (shape factor), depth, polarization angle, and electric dipole moment of a buried structure from residual self-potential (SP) anomalies. The method is based on defining the anomaly value at the origin and four characteristic points and their corresponding distances on the anomaly profile. The problem of shape determination from residual SP anomaly has been transformed into the problem of finding a solution to a nonlinear equation of the form $q = f(q)$. Knowing the shape, the depth, polarization angle and the electric dipole moment are determined individually using three linear equations. Formulas have been derived for spheres and cylinders. By using all possible combinations of the four characteristic points and their corresponding distances, a procedure is developed for automated determination of the best-fit-model parameters of the buried structure from SP anomalies.

The method was applied to synthetic data with 5% random errors and tested on a field example from Colorado. In both cases, the model parameters obtained by the present method, particularly the shape and depth of the buried structures are found in good agreement with the actual ones. The present method has the capability of avoiding highly noisy data points and enforcing the incorporation of points of the least random errors to enhance the interpretation results.

Key words: SP data, shape and depth solutions, numerical methods, noise.

1. Introduction

The self-potential (SP) method is based upon measuring the spontaneous or natural electrical potentials developed in the earth's surface. Different electrical potentials are recognized. Electrokinetic, or streaming, potential is due to the flow of a fluid with certain electrical properties passing through a pipe or porous medium with different electrical properties (Ahmed, 1961). Liquid-junction, or diffusion, potential is caused by the displacement of ionic solutions of dissimilar concentrations (Reynolds, l997). Mineralization, or electrolytic contact, potential is produced at the surface of a conductor with another medium (Sato and Mooney, 1960). Nernst, or shale, potential occurs when similar conductors have a solution of differing concentrations about them (Telford *et al.,* l990). Each of these polarization mechanisms is responsible for an electrical field at the

[1] Geophysics Department, Faculty of Science, Cairo University, Giza, Egypt.
E-mail: sayed5005@yahoo.com

ground surface, the so-called self-potential anomaly. Mineralization potentials have usually been the main interest when prospecting with the self-potential method. They are associated with sulfides of metals, with graphite, and sometimes with the metal oxides such as magnetite.

One of the most important exploration problems is estimating the shape and depth of a buried structure. Different methods have been developed by many workers to determine the shape and the depth of the buried structure from residual self-potential data. The methods generally fall into one of two categories. The first category includes 2-D and 3-D continuous modeling and inversion methods (Guptasarma, l983; Furness, l992; Shi and Morgan, l996; Patella, l997 and Revil *et al*., 2001). However, the drawback of these algorithms is that they cannot be used to interpret a self-potential anomaly profile of a short length. The second category includes fixed simple geometry methods, in which the sphere, horizontal-cylinder and vertical-cylinder models determine the shape and depth of the buried structure from residual SP anomalies. The advantage of the fixed geometry methods over 2-D and 3-D continuous and inversion methods is that they do not require current density, resistivity, and depth information obtained from geological and/or geophysical data, and they can be applied if little or no factual information other than the SP data is available. For interpreting simple source bodies, fixed geometry methods can be both fast and accurate.

Several graphical and numerical fixed geometry methods have been developed by many workers to determine the model parameters (shape, depth, polarization angle, and electric dipole moment) of the buried structure from residual SP anomalies. The methods include, for examples, use of characteristic points, distances, curves and nomograms (Yungul, 1950; Banerjee, 1971; Fitterman, 1979; Bhattacharya and Roy, 1981; Atchuta Rao and Ram Babu, 1983; Ram Babu and Atchuta Rao, 1988), least-squares techniques (Abdelrahman and Sharafeldin, 1997; El-Araby, 2004, and Abdelrahman *et al*., 1997a, 2003, 2004, 2006a-b and 2008), Fourier analysis and wave number domain (Atchuta Rao *et al*., 1982; Roy and Mohan, 1984), window-curves methods (Abdelrahman *et al*., 1997b, 1998, 2003, and 2009). On the other hand, the drawback with most of the previous graphical and numerical methods is that they cannot determine the four model parameters from all data points of the SP anomaly profile.

In this paper, we present a new numerical method to obtain the shape (shape factor), depth, polarization angle, and electric dipole moment from residual SP anomalies caused by simple geometric bodies. The accuracy of the result obtained by this procedure depends upon the accuracy to which the residual anomaly can be separated from SP data. Also, the accuracy of the result of the present method depends on the extent to which the source body conforms to one of the assumed geometries. A scheme for analyzing the SP data has been formulated for determining the best-fit-model parameters of the causative source.

The method is applied to synthetic data with random errors and tested on a field example from Colorado.

2. The Method

Following YUNGUL (1950) and BHATTACHARYA and ROY (1981), the SP anomaly expression, V, produced by most polarized structures is given by the following function

$$V(x_i, z, \theta, q) = K \frac{x_i \cos\theta + z \sin\theta}{(x_i^2 + z^2)^q}, \quad i = 1,\ 2,\ 3, \ldots, N, \tag{1}$$

where z is the depth of the body, x_i is the position coordinate, K is the electric dipole moment, θ is the polarization angle, and q is the shape factor. As examples, the shape factors for a sphere, horizontal cylinder, and a semi-infinite vertical cylinder are 1.5, 1.0, and 0.5, respectively.

At the origin ($x_i = 0$), *equation (1) gives the following relationship*

$$V(0) = Kz^{1-2q} \sin\theta, \tag{2}$$

where $V(0)$ is the anomaly value at the origin.

Substituting equation (2) into equation (1) we obtain the following equation

$$V(x_i, z, \theta, q) = V(0) z^{2q-1} \frac{x_i \cot\theta + z}{(x_i^2 + z^2)^q}. \tag{3}$$

For all shapes, equation (3) gives the following values at $x_i = \pm N$:-

$$V(N) = V(0) z^{2q-1} \left[\frac{N \cot\theta + z}{(N^2 + z^2)^q}\right], \tag{4}$$

and

$$V(-N) = V(0) z^{2q-1} \left[\frac{-N \cot\theta + z}{(N^2 + z^2)^q}\right]. \tag{5}$$

where V(N) and V(-N) are the anomaly values at two symmetrical points around the origin.

From equations (4) and (5), we obtain the following simple linear equation for z:

$$z = N \sqrt{\frac{F^{1/q}}{1 - F^{1/q}}}. \tag{6}$$

where

$$F = \frac{V(N) + V(-N)}{2V(0)},$$

Also, from equations (4) and (5), we obtain the following equation for z in case that $x_i = \pm M$:

$$z = M \sqrt{\frac{D^{1/q}}{1 - D^{1/q}}}, \tag{7}$$

where

$$D = \frac{V(M) + V(-M)}{2V(0)},$$

and where V(M) and V(−M) are the anomaly values at two symmetrical points around the origin.

Using equations (6) and (7), we obtain the following nonlinear equation for q,

$$q = \ln\left(\frac{D}{F}\left[\frac{1 - F^{1/q}}{1 - D^{1/q}}\right]\right) \Big/ 2\ln\frac{M}{N}, \quad M \neq N. \tag{8}$$

Equation (8) can be solved for q using the standard methods for solving nonlinear equations. Here, equation (8) is solved by a simple iteration method (Demidovich and Maron, 1973; Press *et al.*, 1986). The iterative form of equation (8) is given as

$$qf = f(q_j), \tag{9}$$

where q_j is the initial shape factor and q_f is the revised shape factor; q_f will be used as the q_j for the next iteration. The iteration stops when $|q_f - q_j| \leq e$, where e is a small predetermined real number close to zero. The shape is determined by solving one nonlinear equation in q. Any initial guess for q works well because there is always one global minimum. Theoretically, two different values of N and M are enough to determine the shape. In practice, more than two values of N and M are preferable because of the presence of noise in the data.

Again, using equations (4) and (5), the polarization angle (θ) can be determined from the following equation

$$\theta = \tan^{-1}\left[\frac{G(N^2 + z^2)^q}{Nz^{2q-1}}\right], \tag{10}$$

where

$$G = \frac{V(N) - V(-N)}{2V(0)}.$$

Finally, knowing q, z, and θ, the electric dipole moment (K) can be obtained from equation (1) and is given by the following linear equation:

$$K = \frac{S(N^2 + z^2)^q}{2z \sin\theta}, \tag{11}$$

where

$$S = (V(N) + V(-N)).$$

For each N and M value, we compute the values of the four model parameters q, z, θ and K from equations (8), (6), (10) and (11), respectively. Theoretically, the anomaly values at the origin and any two N and M distances are just enough to determine the four model parameters (q, z, θ, and K). However, in practice, it is recommended to use all

possible combinations of N and M values to determine the most appropriate source parameters solutions from all SP data. We then measure the goodness of fit between the observed and computed SP data for each set of solutions. The simplest way to compare two SP profiles is to compute the root-mean-sum-squared differences (rms) between the observed values and the values computed from estimated values of q, z, (θ), and K. The model parameters which give the least root-mean-sum-squares differences are the best. In this way, we can select the best-fit source parameters solutions from all SP data.

An automated interpretation scheme based on the above equations for analyzing field data is illustrated in Figure 1.

Up to this stage, we have assumed knowledge of the origin when applying the present method. In practice, a field traverse will have an arbitrary origin in which case the position of the structure ($x = 0$) in the equation must first be determined. In most cases, the maximum and minimum values of the profile can be used to determine the correct location $x = 0$. A straight line joining the maximum to the minimum of the profile will intersect the anomaly curve at the point $x = 0$ (STANLEY, l977).

3. Theoretical Examples

Three self-potential anomalies are computed. The model equations are:

$$\Delta V_1(x_i) = -100\frac{x_i \cos 30^\circ + 2 \sin 30^\circ}{(x_i^2 + 2^2)^{0.5}}, \tag{12}$$

(Semi-infinite vertical cylinder model)

$$\Delta V_2(x_i) = -300\frac{x_i \cos 45^\circ + 3 \sin 45^\circ}{(x_i^2 + 3^2)}, \tag{13}$$

(Horizontal cylinder model)

$$\Delta V_3(x_i) = -4500\frac{x_i \cos 60^\circ + 5 \sin 60^\circ}{(x_i^2 + 5^2)^{1.5}}. \tag{14}$$

(Sphere model)

The three self-potential fields are given in Figures 2–4. Each anomaly profile was computed at 15 data points from -7 m to $+7$ m with a sampling interval of 1 m.

To test the stability of our method in the presence of noise, each computed self-potential anomaly $\Delta V(x_i)$ was contaminated with random errors with a noise level of 5 mV using the following equation

$$\Delta V \text{ rand}(x_i) = \Delta V(x_i) + 5(\text{RAND(i)} - 0.5), \tag{15}$$

where ΔV rand(x_i) is the contaminated anomaly value at x_i and RAND(i) is a pseudo-random number whose range is (0, 1). The interval of the pseudo-random number is an open interval, i.e., it does not include the extremes 0 and 1.

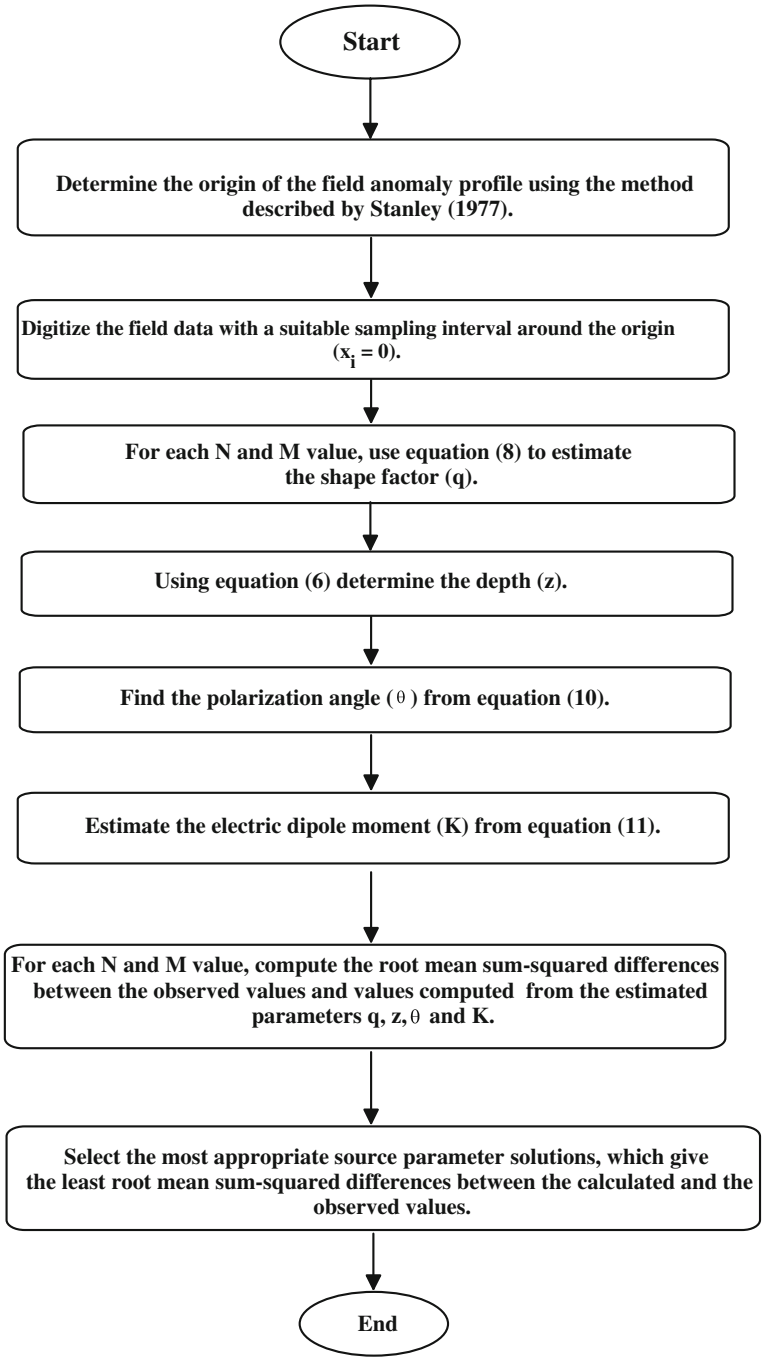
Start
Determine the origin of the field anomaly profile using the method described by Stanley (1977).
Digitize the field data with a suitable sampling interval around the origin ($x_i = 0$).
For each N and M value, use equation (8) to estimate the shape factor (q).
Using equation (6) determine the depth (z).
Find the polarization angle (θ) from equation (10).
Estimate the electric dipole moment (K) from equation (11).
For each N and M value, compute the root mean sum-squared differences between the observed values and values computed from the estimated parameters q, z, θ and K.
Select the most appropriate source parameter solutions, which give the least root mean sum-squared differences between the calculated and the observed values.
End

◀

Figure 1
Generalized scheme for automated shape, depth, polarization angle, and electric dipole moment estimation.

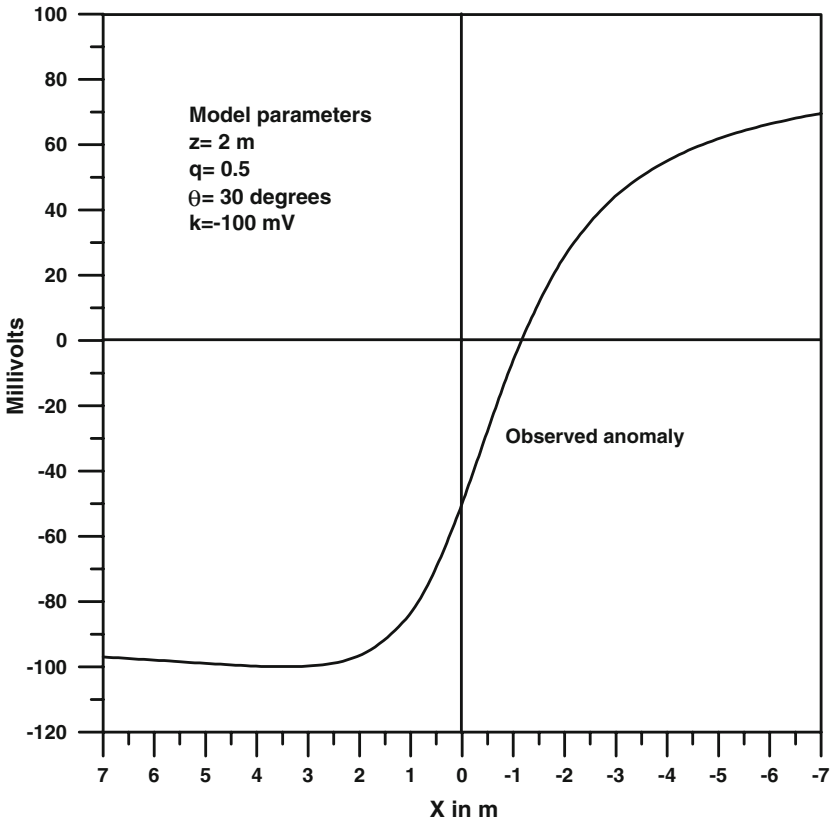

Figure 2
Self-potential anomaly (ΔV_1) of a buried vertical cylinder model as obtained from equation (12).

Numerical results for the three cases including vertical cylinder, horizontal cylinder, and sphere models are shown in Tables 1–3, respectively. In these tables, we have displayed only the results of the cases of N and M values where the rms difference between the modelled and observed data is less than 2 mV. In this way, we can pick out the subset of models that fits the data within some small variation from minimum. We then calculate the mean and the standard deviation of the parameters.

It was numerically verified that equations (8), (6), (10), and (11) give exact values of the four model parameters when synthetic data are analyzed. On the other hand, when the data are noisy, the best-fit-model parameters (optimum set) are obtained when $N = \pm 7$ m

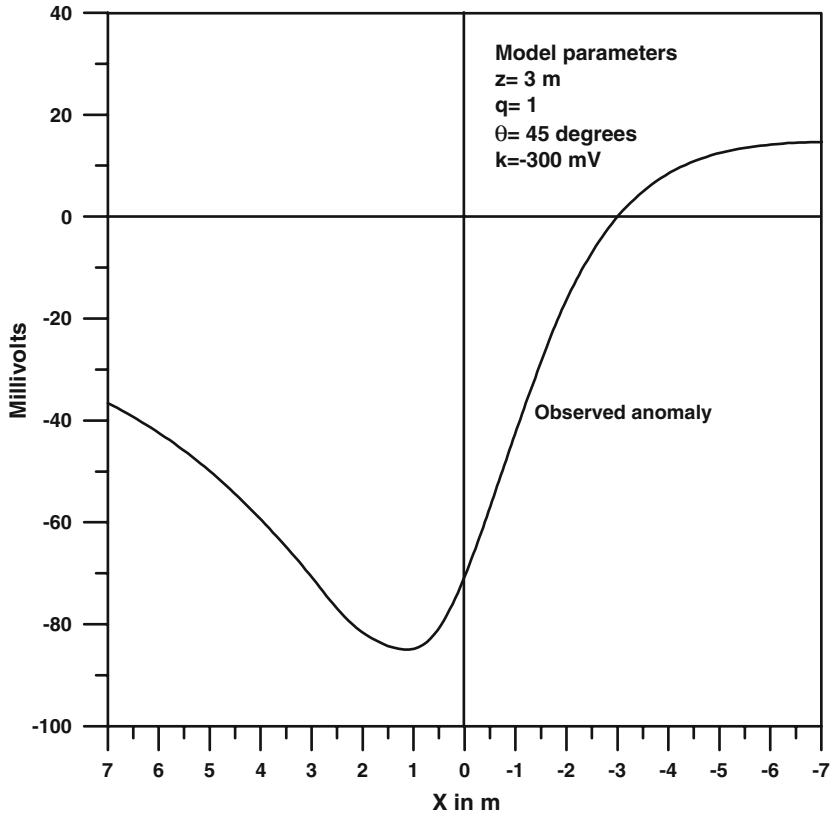

Figure 3
Self-potential anomaly (ΔV_2) of a buried horizontal cylinder model as obtained from equation (13).

and M = ± 1 m for the vertical cylinder model (Table 1), N = ±2 m and = ±6 m for the horizontal cylinder model (Table 2), and N = ±6 m and M = ±7 m f or the sphere model (Table 3). The percentage of error in the shape factor is 0.11, 4.46, and 2.39 for the three models, respectively, whereas the percentage of error in the depth parameter is 5.28, 0.32, and 2.22, respectively. The maximum error in the polarization angle is 2.56% (Table 2), whereas the maximum error in the electric dipole moment is about 15% (Table 3), for the three models. Generally, the percentage of error in the optimum sets is low because the method avoids highly noisy data points and enforcing the incorporation of points of the least random errors to enhance the interpretation results.

On the other hand, the sets of the mean values of the model parameters shown in Tables 1–3 have generally large values of percentage of error and root-mean-sum-squared errors between the observed values and the values computed from the estimated average parameters q, z, θ, and K. This is because of the fact that the set of mean values is

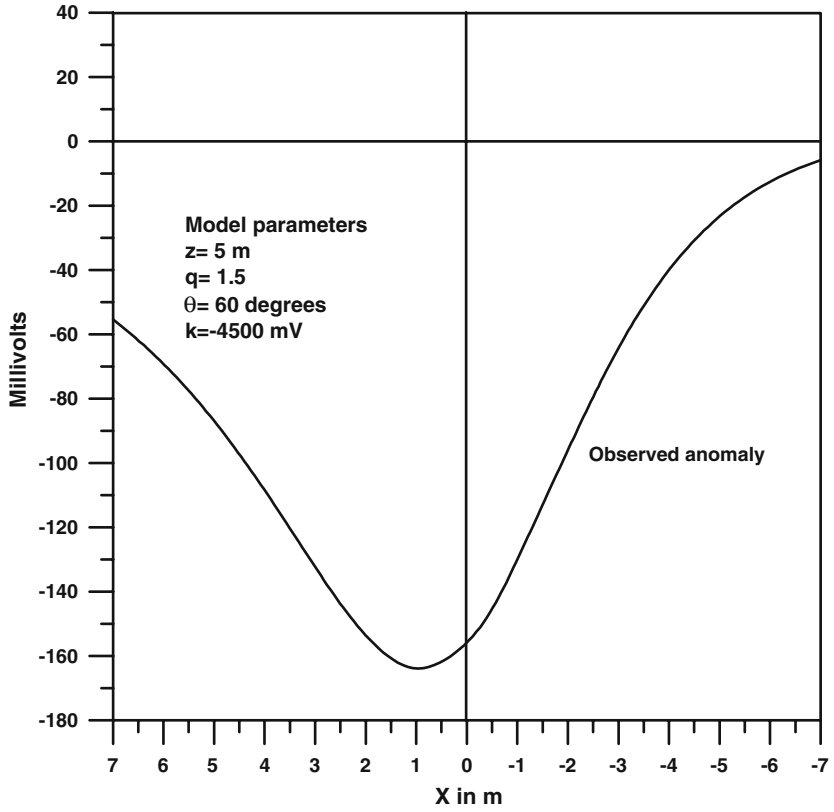

Figure 4
Self-potential anomaly (ΔV_3) of a buried sphere model as obtained from equation (14).

influenced by all noisy data points whereas the optimum set obtained using the present method is computed only from the least noisy data points.

Good results are obtained by using the present algorithm, particularly for shape and depth estimation, because our technique has the capability of avoiding highly noisy data points and enforcing the incorporation of points of the least random errors to enhance the interpretation results, particularly when applied to field data.

4. *Field Example*

A self-potential anomaly profile along line 22 of the map of self-potential data over a Malachite Mine, Jefferson County, Colorado (DOBRIN, 1960, Figures 19–25, p. 426) is shown in Figure 5. The SP anomaly measurements were performed and described by HEILAND *et al*. (1945). This anomaly profile is due to a nearly vertical cylindrical massive

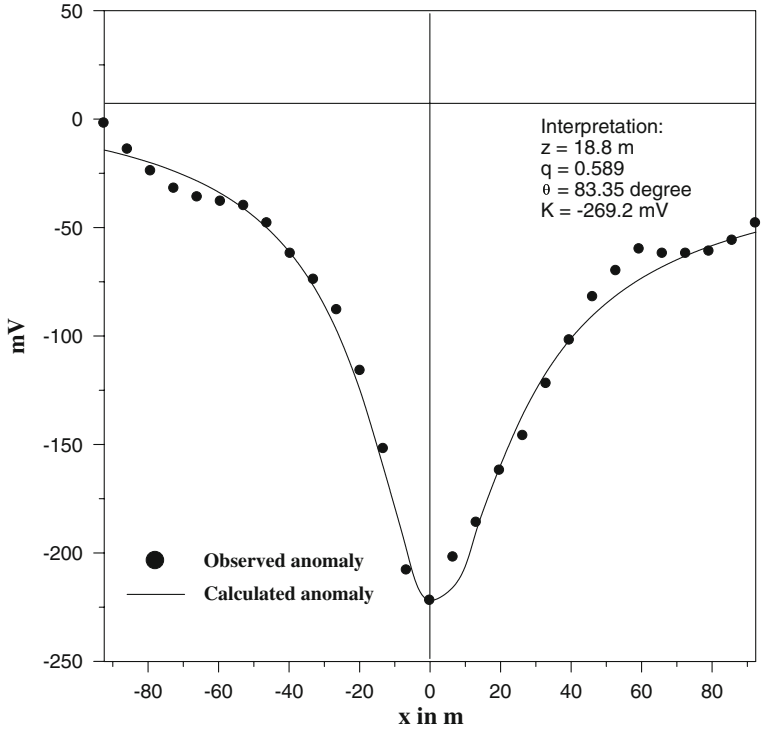

Figure 5
Measured and calculated SP anomaly over a Malachite Mine, Jefferson County, Colorado (Dobrin, 1960, Figures 19–25, p. 426).

Table 1

Numerical results of the present method applied to the vertical cylinder synthetic example ($q = 0.5$, $z = 2$ m, $\theta = 30$ degrees, $k = -100$ mV, profile length = 14 m, sampling interval = 1 m) with 5% random noise (best fit in bold)

N (m)	M (m)	Shape factor (q)	% of error in q	Depth z (m)	% of error in z	Polarization angle θ (degree)	% of error in θ	Electric dipole moment K (mV)	% of error in K	Rms (mV)
2	6	0.48	−3.68	1.77	−11.32	31.75	5.84	−93.03	−6.97	1.57
2	7	0.47	−5.28	1.75	−12.40	32.07	6.89	−91.44	−8.56	1.60
3	4	0.48	−3.68	1.77	−11.32	31.75	5.84	−93.03	−6.97	1.57
3	5	0.50	−0.89	2.07	3.38	30.13	0.44	−98.96	−1.04	1.89
5	3	0.50	−0.89	2.07	3.38	30.20	0.68	−98.74	−1.26	1.88
5	6	0.50	−0.89	2.07	3.38	30.20	0.68	−98.74	−1.26	1.88
6	1	0.51	2.12	1.92	−4.09	29.70	−1.01	−102.32	2.32	1.64
6	2	0.48	−3.68	1.77	−11.32	31.67	5.56	−93.25	−6.75	1.57
7	**1**	**0.50**	**−0.11**	**1.89**	**−5.28**	**30.66**	**2.19**	**−97.99**	**−2.01**	**1.40**
7	2	0.47	−5.28	1.75	−12.40	32.66	8.87	−89.95	−10.05	1.99
Mean value		0.49	2.00	1.88	6.00	31.08	3.60	−95.75	4.25	1.49
SD (mV)		0.01		0.14		1.01		4.08		

Table 2

Numerical results of the present method applied to the horizontal cylinder synthetic example (q = 1, z = 3 m, θ = 45 degrees, k = −300 mV, profile length = 14 m, and sampling interval = 1 m) with 5% random noise (best fit in bold)

N (m)	M (m)	Shape factor (q)	% of error in q	Depth z (m)	% of error in z	Polarization angle θ (degree)	% of error in θ	Electric dipole moment K (mV)	% of error in K	Rms (mV)
1	4	0.79	−21.00	2.50	−16.64	50.81	12.90	−155.26	−48.25	1.82
1	6	0.81	−18.63	2.54	−15.31	50.36	11.91	−164.84	−45.05	1.65
2	4	1.09	8.53	3.25	8.17	43.99	−2.23	−403.88	34.63	1.72
2	5	0.93	−6.86	2.96	−1.19	46.59	3.52	−248.60	−17.13	1.21
2	**6**	**0.96**	**−4.46**	**3.01**	**0.32**	**46.15**	**2.56**	**−267.47**	**−10.84**	**1.06**
2	7	1.05	4.56	3.18	5.84	44.62	−0.84	−355.16	18.39	1.37
3	4	0.90	−9.76	2.80	−6.61	47.67	5.93	−219.15	−26.95	1.11
3	5	0.80	−20.00	2.57	−14.47	50.16	11.46	−162.11	−45.96	1.86
3	6	0.87	−13.30	2.72	−9.26	48.49	7.75	−196.95	−34.35	1.26
3	7	0.99	−1.12	2.99	−0.39	45.83	1.83	−287.46	−4.18	1.33
4	2	1.09	8.53	3.25	8.17	41.72	−7.29	−421.52	40.51	1.79
4	3	0.90	−9.76	2.80	−6.61	45.92	2.05	−225.51	−24.83	1.98
4	7	1.02	2.13	3.10	3.19	43.07	−4.30	−336.33	12.11	1.72
5	2	0.93	−6.86	2.96	−1.19	46.81	4.03	−247.68	−17.44	1.19
5	3	0.80	−20.00	2.57	−14.47	50.91	13.12	−160.38	−46.54	1.78
5	6	1.03	3.18	3.25	8.20	44.22	−1.74	−354.74	18.25	1.27
6	1	0.81	−18.63	2.54	−15.31	51.25	13.89	−162.77	−45.74	1.96
6	2	0.96	−4.46	3.01	0.32	46.45	3.23	−266.13	−11.29	1.12
6	3	0.87	−13.30	2.72	−9.26	49.31	9.58	−194.49	−35.17	1.48
6	4	0.85	−15.07	2.66	−11.24	49.94	10.97	−183.14	−38.95	1.62
6	5	1.03	3.18	3.25	8.20	44.29	−1.58	−354.28	18.09	1.27
6	7	0.90	−9.76	2.80	−6.61	45.92	2.05	−225.51	−24.83	1.98
7	2	1.05	4.56	3.18	5.84	43.70	−2.88	−361.05	20.35	1.10
7	3	0.99	−1.12	2.99	−0.39	45.44	0.98	−289.35	−3.55	1.17
7	4	1.02	2.13	3.10	3.19	44.43	−1.27	−328.08	9.36	1.08
7	6	1.03	3.18	3.25	8.20	44.22	−1.74	−354.74	18.25	1.27
Mean value		0.94	−6.00	2.92	−2.67	46.63	3.62	−266.41	−11.20	3.34
SD (mV)		0.09		0.26		2.74		82.82		

sulphide ore body approximately 11 m wide and buried at a depth of about 16.5 m (HEILAND *et al*., 1945). The anomaly profile was digitized at an interval of 6.6 m. The method was applied to the anomaly profile using a sampling interval of 13.2 m to determine the model parameters of the buried structure using all successful combinations of N and M values. Then we computed the root-mean-sum-squared error (rms) between the observed values and the values computed from estimated parameters q, z, θ, K for each N and M value. The results are shown in Table 4 for the cases of N and M values where the rms difference between the modelled and observed data are less than 8 mV. Also we computed the set of mean values and standard deviations. The set of mean values of the model parameters is rejected because it has a larger rms value (7.41 mV) than the rms value of the optimum set (7.13 mV). The optimum set is given at N = ±39.6 m and

Table 3

Numerical results of the present method applied to the sphere synthetic example ($q = 1.5$, $z = 5$ m, $\theta = 60$ degrees, $k = -4500$ mV, profile length = 14 m and sampling interval = 1 m) with 5% random noise (best fit in bold)

N (m)	M (m)	Shape factor (q)	% of error in q	Depth z (m)	% of error in z	Polarization angle θ (degree)	% of error in θ	Electric dipole moment K (mV)	% of error in K	Rms (mV)
1	5	1.38	−7.91	4.62	−7.57	61.78	2.97	−2627.69	−41.61	1.72
1	6	1.19	−20.61	4.28	−14.34	63.56	5.93	−1299.09	−71.13	1.99
1	7	1.36	−9.38	4.58	−8.33	61.98	3.30	−2417.10	−46.29	1.59
2	5	1.34	−10.98	4.51	−9.81	62.00	3.34	−2185.82	−51.43	1.75
2	7	1.33	−11.23	4.50	−9.94	62.04	3.40	−2155.64	−52.10	1.73
3	4	1.49	−0.94	4.97	−0.68	60.38	0.64	−4227.19	−6.06	1.31
3	5	1.30	−13.36	4.49	−10.20	62.51	4.19	−1940.20	−56.88	1.41
3	6	1.29	−13.86	4.57	−8.51	62.36	3.94	−1957.13	−56.51	1.91
3	7	1.52	1.20	5.03	0.56	60.08	0.13	−4819.32	7.10	1.34
4	3	1.49	−0.94	4.97	−0.68	59.79	−0.36	−4252.68	−5.50	1.42
4	5	1.48	−1.07	4.89	−2.12	60.52	0.87	−4075.82	−9.43	1.32
4	7	1.53	1.82	5.05	1.07	59.35	−1.08	−5056.02	12.36	1.44
5	1	1.38	−7.91	4.62	−7.57	61.76	2.94	−2628.17	−41.60	1.71
5	2	1.34	−10.98	4.51	−9.81	62.34	3.91	−2178.99	−51.58	1.79
5	4	1.46	−2.39	4.89	−2.22	61.45	2.41	−3786.17	−15.86	1.41
5	7	1.33	−11.54	4.49	−10.22	62.45	4.09	−2106.68	−53.18	1.80
6	1	1.19	−20.61	4.28	−14.34	64.36	7.27	−1290.22	−71.33	1.91
6	3	1.29	−13.86	4.57	−8.51	62.86	4.77	−1948.30	−56.70	1.86
6	4	1.22	−18.75	4.37	−12.70	63.94	6.56	−1443.47	−67.92	1.86
6	7	**1.46**	**−2.39**	**4.89**	**−2.22**	**60.84**	**1.40**	**−3808.33**	**−15.37**	**1.16**
7	3	1.52	1.20	5.03	0.56	60.65	1.08	−4792.16	6.49	1.56
7	4	1.53	1.82	5.05	1.07	60.53	0.88	−4996.39	11.03	1.57
7	6	1.48	−1.07	4.89	−2.12	60.52	0.87	−4075.82	−9.43	1.32
Mean value		1.39	−7.33	4.69	−6.20	61.65	2.75	−3046.45	−32.29	2.58
SD (mV)		0.11		0.26		1.33		1285.71		

Table 4

Numerical results of the present method applied to the field example (best fit in bold)

N (m)	M (m)	Shape factor (q)	Depth z (m)	Polarization angle θ (degree)	Electric dipole moment K (mV)	rms (mV)
39.6	**26.4**	**0.59**	**18.82**	**83.35**	**−269.23**	**7.13**
39.6	66	0.57	18.19	83.57	−257.42	7.19
39.6	79.2	0.52	16.36	84.21	−230.25	7.72
79.2	13.2	0.50	15.53	85.09	−223.37	7.76
79.2	26.4	0.54	17.45	84.49	−240.15	7.87
79.2	39.6	0.52	16.36	84.83	−230.01	7.68
Mean value		0.54	17.12	84.26	−241.74	7.41
SD (mV)		0.03	1.25	0.69	17.95	

M = ±26.4 m. The best-fit-model parameters are q = 0.59, z = 18.82 m, $\theta = 83.4°$ and K = 296.2 mV (Fig. 5). This suggests that the shape of the buried structure resembles a 3-D semi-infinite vertical cylinder model buried at a depth of 18.8 m. The shape and the depth to the top of the ore body obtained by the present method agrees very well with those obtained from drilling information (HEILAND *et al*., 1945; DOBRIN, 1960).

5. Conclusions

The problem of determining the appropriate shape, depth, polarization angle, and electric dipole moment of a buried structure from the residual SP data of a short or a long profile length can be solved using the present method. A simple and rapid approach is formulated to use the anomaly values at the origin and two pairs of measured data points (±N and ±M). The repetition of the method using all possible combinations of such pairs of measured points will lead to the best-fitting model. This happens when these two pairs of points contain the least amount of noise in the entire set of measured data. It is also emphasized that the calculated SP anomaly of a set of mean values of the model parameters obtained by the present method does not necessarily guarantee it matches the observed anomaly values when the data contain measurement errors. The advantages of this method over previous graphical and numerical techniques used to interpret SP data are: (1) all the four model parameters can be obtained from all observed data, (2) the method is automatic, and (3) the method is less sensitive to errors in the SP anomaly. Moreover, the advantage of the present method over the least-squares method is that the method does not require computation of analytical or numerical derivatives with respect to the model parameters. It is also emphasized that the present method can be used to gain geologic insight concerning the subsurface, as illustrated in the field example.

Finally, in view of the above facts, we envisage the application of this method in solving various problems related to potential field data interpretation in the future.

Acknowledgements

The authors thank the editors and a capable reviewer for their excellent suggestions and thorough review that enhanced our original manuscript.

References

ABDELRAHMAN, E. M., EL-ARABY, T. M., and ESSA, K. S. (2009), *Shape and depth determinations from second moving average residual self-potential*, J. Geophys. Eng. *6*, 43–52.

ABDELRAHMAN, E. M., AMMAR, A. A., HASSANEIN, H. I. and HAFEZ, M. A. (1998), *Derivative analysis of SP anomalies*, Geophys. *63*, 890–497.

ABDELRAHMAN, E. M., AMMAR, A. A., SHARAFELDIN, S. M., and HASSANEIN, H. I. (1997b), *Shape and depth solutions from numerical horizontal self-potential gradients*, Appl. Geophys. *36*, 31–43.

ABDELRAHMAN, E. M. and SHARAFELDIN, S. M. (1997), *A least-squares approach to depth determination from residual self-potential anomalies caused by horizontal cylinders and spheres*, Geophys. *62*, 44–48.

ABDELRAHMAN, E. M., EL-ARABY, H. M, HASSANEEN, A. GH., and HAFEZ, M. A. (2003), *New methods for shape and depth determinations from SP data*, Geophys. *68*, 1202–1210.

ABDELRAHMAN, E. M., EL-ARABY, T. M., AMMAR, A. A., and HASSANEIN, H. I. (1997a), *A least-squares approach to shape determination from residual self-potential anomalies*, Pure Appl. Geophys. *150*, 121–128.

ABDELRAHMAN, E. M., ESSA, K. S., ABO-EZZ, E. R., and SOLIMAN, K. S. (2006a), *Self-potential data interpretation using standard deviation of depths computed from moving average residual anomaly*, Geophys. Prosp. *54*, 1–16.

ABDELRAHMAN, E. M., ESSA, K. S., ABO-EZZ, E. R., SOLIMAN, K. S., and EL-ARABY, T. M. (2006b), *A least-squares depth–horizontal position curves method to interpret residual SP anomaly profile*, J. Geophys. Eng. *3*,252–259.

ABDELRAHMAN, E. M., ESSA, K. S., ABO-EZZ, E. R., SULTAN, M., SAUCK, W. A., and GHARIEB, A. G. (2008), *New least-squares algorithm for model parameters estimation using self-potential anomalies*, Computers and Geosciences, *43*, 1569–1576.

ABDELRAHMAN, E. M., SABER, H. S., ESSA, K. S., and FOUDA, M. A. (2004), *A least-squares approach to depth determination from numerical horizontal self-potential gradients*, Pure Appl. Geophys. *161*, 399–411.

AHMED, M. U. (l961), *A laboratory study of streaming potentials*, *Geophys. Prosp. 12*(1), 49–64.

ATCHUTA RAO, D. and RAM BABU, H. V. (1983), *Quantitative interpretation of self-potential anomalies due two-dimensional sheet-like bodies*, Geophys. *48*, 1659–1664.

ATCHUTA RAO, D., RAM BABU, H. V., and SILVAKUMAR SINHA, G. D. J. (1982), *A Fourier transform method for the interpretation of self-potential anomalies due to the two-dimensional inclined sheets of finite depth extent*, Pure Appl. Geophys. *120*, 365–374.

BANERJEE, B. (1971), *Quantitative interpretation of self-potential anomalies of some specific geometric bodies*, Pure Appl. Geophys. *90*, 138–152.

BHATTACHARYA, B. B. and ROY, N. (1981), *A note on the use of nomograms for self-potential anomalies*, Geophys. Prosp. *29*, 102–107.

DEMIDOVICH, B. P. and MARON, I. A. (1973),*Computational mathematics*, Mir. Publ.

DOBRIN, M. B. *Introduction to Geophysical Prospecting*. Mc Graw Hill Book Company, Inc., New York 1960.

EL-ARABY, H. M. (2004), *A new method for complete quantitative interpretation of self-potential anomalies*, J. Appl. Geophys. *55*, 211–224.

FITTERMAN, D. V. (1979), *Calculations of self-potential anomalies near vertical contacts,* Geophys. *44*, 195–205.

FURNESS, P. (1992), M*odeling spontaneous mineralization potentials with a new integral equation*, J. Appl. Geophys. *29*, 143–155.

GUPTASARMA, D. (1983), *Effect of surface polarization on resistivity modelling*, Geophys. *48*, 98–106.

PATELLA, D. (1997), *Introduction to ground surface Self-Potential tomography*, Geophys. Prosp. *45*, 653–681.

PRESS, W. H., FLANNERY, B. P., TEUKOLSKY, S. A. and VETTERLING, W. T. *Numerical Recipes, The Art of Scientific Computing* (Cambridge: Cambridge University Press, 1986).

RAM BABU, H. V. and ATCHUTA RAO, D. (1988), *A rapid graphical method for the interpretation of the self-potential anomaly over a two-dimensional inclined sheet of finite depth extent,* Geophys. *53*, 1126–1128.

REVIL, A., EHOUARNE, L., and THYREAULT, E. (2001), *Tomography of self-potential anomalies of electrochemical nature*, Geophys. Res. Lett. *28*, 4363–4366.

REYNOLDS, M. J. *An introduction to Applied and Environmental Geophysics* (John Wiley & Sons Ltd, England, 1997).

ROY, S. V. S. and MOHAN, N. L. (1984). *Spectral interpretation of self-potential anomalies of some simple geometric bodies*, Pure Appl. Geophys. *78*, 66–77.

SATO, M. and MOONEY, H. M. (1960), *The electrochemical mechanism of sulfide self-potentials*, Geophy. *25*, 226–249.

SHI, W. and MORGAN, F. D. (1996), *Non –uniqueness in self-potential in version,* 66th Ann. Internat. Mtg. Soc. Expt. Geophys. Extanded Abstracts, 950–953.

STANLEY, J. M. (1977), *Simplified magnetic interpretation of the geologic contact and thin dike*, Geophys. *42*, 1236–1240.

TELFORD, W. M., GELDERT, L. P., and SHERIFF, R. A., *Applied Geophysics*, 2nd Ed. (Cambridge University Press 1990).

YUNGUL, S. (1950), *Interpretation of spontaneous polarization anomalies caused by spherical ore bodies*, Geophys. *15*, 237–246.

(Received April 26, 2008, accepted May 6, 2009)
Published Online First: August 20, 2009